Review of Capacity Fade Models for Lithium-ion Batteries -- Effect of Mechanisms on Numerical Implementation

Mengdi Fan

A thesis

submitted in partial fulfillment of the

requirements for the degree of

Master of Science in Chemical Engineering

University of Washington

2018

Committee:

Venkat R. Subramanian

Daniel Schwartz

Program Authorized to Offer Degree:

Chemical Engineering

University of Washington

Abstract

Review of Capacity Fade Models for Lithium-ion Batteries -- Effect of Mechanisms on Numerical Implementation

Mengdi Fan

Chair of the Supervisory Committee:
Research Professor Venkat R. Subramanian
Department of Chemical Engineering

Lithium-ion battery applications, such as EVs and PHEVs, require long battery life. However, capacity fade always occurs due to unwanted side reactions including electrolyte oxidation at the positive electrode, electrolyte decomposition processes, and the formation of the Solid-Electrolyte Interphase (SEI) layer[1]. To simulate the capacity fade, different models have been proposed in the literature[2]-[4].

In this work, the capacity fade is modeled by assuming the SEI layer formation to be the dominant mechanism. Even among SEI layer models, several different expressions have been

used in many papers[5]-[8]. In most cases, the solid particles are assumed to be spherical, and the intercalation process is modeled using Fick's law of diffusion in the radial direction. In this work, the SEI-forming side reaction based on the Single Particle Model (SPM) is studied. Three models are compared with different charging rates cycling study.

For solving the solid-phase diffusion in the radial-dimension, many efficient mathematical algorithms of reformulation and simulation have been proposed in the past[9]-[12]. We address how those different SEI layer growth expressions affect the numerical implementation stability. The partial differential equations of the SPM are discretized using the finite difference method in the radial direction and solved in time using the numerical method of lines approaches.

TABLE OF CONTENTS

LIST OF FIGURES

LIST OF TABLES

ACKNOWLEDGEMENTS

The author thanks the Department of Energy (DOE) for providing partial financial support for this work, through the Advanced Research Projects Agency (ARPA-E) award number DE-AR0000275. The author would like to express her sincere appreciation to her advisor Prof. Venkat Subramanian for his guidance and passion in the clean energy field, her group members Caitlin, Seongbeom, Manan, Yanbo, Jerry, Neal, Tae-Jin, Akshay, Surya and Linnette for their care and support.

Chapter 1. INTRODUCTION

1.1 BACKGROUND OF LITHIUM-ION BATTERY

Electric vehicles (EVs) and plug-in hybrid electric vehicles (PHEVs) have several advantages over conventional internal combustion engine (ICE) vehicles. Besides the environment-friendly benefits like lower air pollution and reduction of petroleum consumption, EVs and PHEVs also have lower operating and maintenance costs. However, as far as price concerned, EVs are still not competitive with ICE vehicles even after on century development. The higher rates of EVs are due to the expensive vehicle's battery pack. Among the currently available and planned EVs and PHEVs, the lithium-ion battery chemistry is the most popular one. The cost of the Li-ion EV battery pack, $10,000 per vehicle, accounts for 30-50% of the total vehicle cost[13]. Decreasing the price of the battery is a major way to make the EVs and PHEVs more cost competitive and increase the market share.

For EVs and PHEVs battery, the capacity and power fade are the main reasons why the battery pack needed to be replaced. When EV batteries reach 80% of their nameplate capacity, they must be replaced. Power fade is the loss of cell power caused by increased cell impedance from aging. Capacity fade is defined as the loss of energy storage capacity due to degradation caused by cycling[14]. In short, the capacity and power fade determine the economic and practical value of the battery pack. In order to decrease the battery degradation and to increase the battery lifetime, both experiments and theoretical/numerical works have been implemented to study the capacity and power fade.

To better understand and predict the battery lifetime, the mechanisms which cause battery degradation should be studied first. There are two main categories of battery degradation: calendar aging and cycling aging. The calendar degradation refers to all aging processes that regardless of

charge-discharge cycling. The primary mechanism of calendar aging is the growth of passivation layers at the electrode-electrolyte interface[15]. Conversely, cycling degradation is due to all the cycling processes which are the mechanical strain in the electrode active materials or the lithium plating[15]. Applications which expand a long duration with few life cycles are affected more by calendar life while applications which operated under repeated charge-discharge cycling are influenced more by cycling life. As for EVs and PHEVs, both calendar and cycling aging are essential based on the usage mode.

In Lithium-ion cells, many different internal mechanisms lead to capacity fade. Those mechanisms include the lithium deposition due to overcharge conditions, electrolyte decomposition, active material dissolution, phase changes in the insertion electrode materials, and passive film formation over the electrode and current collector surfaces[1]. Among those mechanisms, the creation of the passive film over the negative electrode, also known as the solid-electrolyte interface (SEI) growth, explains the cell increasing resistance and the active lithium lost. During cycling, especially the charging process, the SEI layer growth side reaction takes place between the anode and the electrolyte. During the first few cycles, the formation of SEI layer consumes lithium which leads to an initial capacity degradation. This layer serves as a protective barrier between the anode and electrolyte during the next cycles which isolates the negative electrode from the electrolyte and reduce the further reaction. However, the continued side reaction during cycling will increase the battery resistance and cause additional capacity and power fade. The SEI layer growth is able to account for overall capacity fade for battery with graphite anode[14].

1.2 Background of Single Particle Model

Different methods have been implemented to simulate battery lifetime performance. Basically, those methods could be separate as statistical approaches and physics-based models. The isothermal single particle model (SPM) is a fundamental physics-based model, which considers each electrode as a single spherical particle. The SPM was first developed by Atlung et al.[16] and used to describe the lithium-ion battery later on. Figure 1.1 is the schematic representation of SPM.

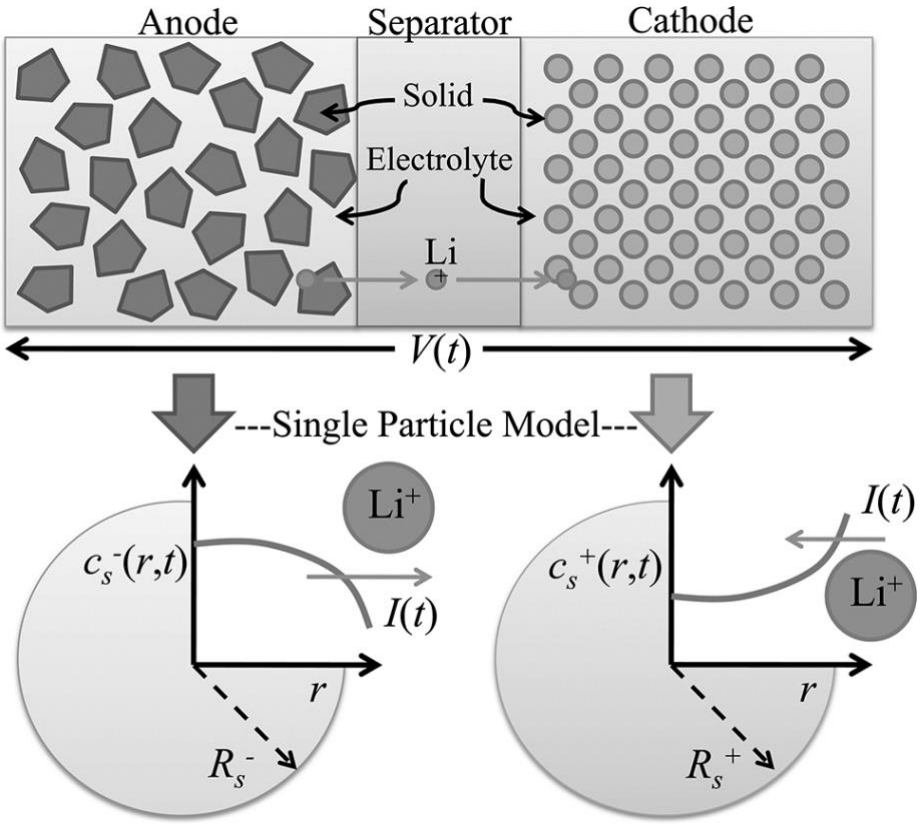

Figure 1.1. Single particle model[17].

The current distribution along the thickness of the electrode is uniform. And this model neglects the solution phase limitation which means the electrolyte potential is not considered and the concentration is constant through the electrolyte phase. Within the electrode solid phases, the diffusion is described by Fick's second law

$$\frac{\partial c_{s,i}}{\partial t} = \frac{1}{r^2}\frac{\partial}{\partial r}\left(D_{s,i} r^2 \frac{\partial c_{s,i}}{\partial r}\right) \qquad i = n, p \tag{1.1}$$

where $c_{s,i}$ is the lithium concentration in the solid phase, t is time, r is the radius direction coordinate, $D_{s,i}$ is the solid phase diffusion coefficient. And the subscript $i = n, p$ refers to anode n and cathode p.

Due to the symmetry, the lithium mass flux at the center of the particle is zero. The two boundary conditions are

$$\left(D_{s,i}\frac{\partial c_{s,i}}{\partial r}\right)_{r=0} = 0 \qquad i = n, p \tag{1.2}$$

$$\left(D_{s,i}\frac{\partial c_{s,i}}{\partial r}\right)_{r=R_i} = -j_i \quad i = n, p \tag{1.3}$$

where j_i is the pore wall flux of lithium at the surface.

The relation between flux and current density for two electrodes are

$$j_i = \frac{i_{int,i}}{F a_i l_i} \qquad i = n, p \tag{1.4}$$

where $i_{int,i}$ is the intercalation current density refer to the interfacial surface area of the anode, F is the Faraday's constant, a_i is the particle surface area to volume, and the $l_i$is the length of the electrode.

The lithium intercalation/deintercalation into the active materials follows Bulter-Volmer kinetics

$$j_n = k_n\left(c_{n,max} - c_{s,Rn}\right)^{0.5} c_{s,Rn}^{0.5}\left\{exp\left(\frac{0.5F\left(\phi_n - U_n - Rsei * i_{app}\right)}{RT}\right) - exp\left(-\frac{0.5F\left(\phi_n - U_n - Rsei * i_{app}\right)}{RT}\right)\right\} \tag{1.5}$$

$$j_p = k_p\left(c_{p,max} - c_{s,Rp}\right)^{0.5} c_{s,Rp}^{0.5}\left\{exp\left(\frac{0.5F\left(\phi_p - U_p\right)}{RT}\right) - exp\left(-\frac{0.5F\left(\phi_p - U_p\right)}{RT}\right)\right\} \tag{1.6}$$

where k_i is the rate constant for lithium intercalation reaction, $c_{i,max}$ is the maximum concentration of lithium inside the active material, $c_{s,Ri}$ is the lithium concentration at the

electrode surface, ϕ_i is the solid-state potential, U_i is the equilibrium potential, R_{sei} is the SEI layer resistance.

The current balance for two electrodes are given below, the current balance for anode includes the side reaction current density

$$-i_{int,p} = i_{app} \qquad i_{int,n} + i_{sei} = i_{app} \tag{1.7}$$

where i_{app} is the Applied current density, i_{sei} is the SEI side reaction current density referred to interfacial surface area of anode.

Chapter 2. REVIEW OF SEI LAYER GROWTH MODELS

In this work, SEI layer growth is assumed to be the primary cause of capacity fade for lithium-ion batteries with graphite negative electrodes according to literature. We focus on how to describe the SEI layer side reaction based on physics-based models. While plenty of SEI formation models have been proposed in the literature, those models emphasize different aspects. In this chapter, we review and compare some typical models. Before going to the models, a review of the SEI layer reaction mechanisms is in order. Firstly, there are different options regarding the reaction scheme for this side reaction. Since the nature of the reaction depends on the solvent type used in the battery electrolyte, some models consider this parasitic reaction as a solvent oxidation side reaction while others assume it is a solvent reduction reaction. Secondly, this side reaction takes place at the lithium intercalation/deintercalation interface, and the experimental data indicates that to describe the capacity fade, both transport limitation and kinetic limitation should be included for the parasitic forming reaction[8]. Finally, the SEI layer is not homogeneous since the initial layer cannot totally support the volume change due to graphite expansion during the following intercalation process. As a result, cracks form in the SEI film. On the basis of the literature, there are some other common assumptions. Most of the literature regard the SEI parasitic reaction only occurs during the charging process and this formation is irreversible.

In this chapter, those models are reviewed that follow the above aspects to give a review of SEI layer generation models. Some models are built on SPM while others utilize the Porous Electrode Pseudo 2D (P2D) model. In here, we mainly concentrate on how they describe the SEI layer formation and apply the mechanisms to SP model.

2.1 REACTION SCHEME

The first attempt to model the side reaction in Li-ion battery is Darling and Newman's[18] solvent oxidation reaction.

Several possible reaction schemes are available in the literature. In 2004, Ramadass and his fellows chose the two-electron reduction of ethylene carbonate (EC) as the SEI layer reaction which formed a mixture of organic and inorganic productions[6]. Eq.2.1 is the reduction reaction.

$$S + 2Li^+ + 2e^- \rightarrow P \tag{2.1}$$

Later in 2004, Ploehn and Ramadass et al. [19] also assumed that one solvent component dominates the two-electron reduction at SEI layer- graphite interface. And they also considered that this dominant component is dilute within the SEI layer which gives $c_s \ll c_p$ as an assumption.

In 2009, Safari et al. considered the lithium ethylene dicarbonate $(CH_2OCO_2Li)_2$ as the SEI layer component. The rate-determining step is the formation of EC radical anions, which is a one-electron reduction reaction[5]. They used dilute solution theory to describe the minor species' transport properties.

Ekstrom et al.[8] published a paper in 2015 in which they proposed a model that further simplifies the SPM approach by assuming that the lithium concentration within the anode active material is uniform.

2.2 CHEMICAL KINETICS

2.2.1 *Kinetic Limited Models*

In Ramadass's[6] work, their first principle model applied the Bulter-Volmer kinetic expression to define the rate of solvent reduction. They assumed that the reduction reaction is irreversible so

a cathodic Tafel approximation is used to simplify the calculation. Solvent diffusion limitation through the SEI layer is not included in this model. The Tafel equation in the model is

$$i_{sei} = -a_n l_n F i0_{sei} e^{-\frac{\alpha_c F}{RT}(\phi_n - U_{sei} - \frac{i_{app} R_{sei}}{anln}])} \tag{2.2}$$

where $i0_{sei}$ is the concentration dependent equilibrium exchange current density, α_c is the cathodic transfer coefficients of electrochemical reaction and the equilibrium potential, U_{sei}, is 0.4V vs Li/Li+.

The resistance of the SEI layer consists of two parts, the initially formed resistance and the resistance due to the products developed during the charging process

$$R_{sei} = R_{0,sei} + Rp, \qquad Rp = \frac{\delta_{sei}}{\kappa_{sei}} \tag{2.3}$$

where $R_{0,sei}$ is the initial resistance.

The SEI film thickness increasing rate is:

$$\frac{\partial \delta_{sei}}{\partial t} = -\frac{i_{sei} M_{sei}}{a_n l_n F \rho_{sei}} \tag{2.4}$$

where δ_{sei} is the SEI film thickness, M_{sei} is the molecular weight of SEI layer, ρ_{sei} is the SEI layer density.

2.2.2 *Diffusion Limited Models*

In the work by Ploehn[19] et al., they treated the SEI parasitic reaction as only diffusion-limited. The SEI layer growth rate is limited by the solvent diffusion through the exist SEI layer alone. And by applying the Fick's second law and dilute theory ($c_s \ll c_p$) assumption, they derived the following equations to describe SEI film formation.

$$\frac{\partial c_e}{\partial t} = D_{sei} \frac{\partial^2 c_e}{\partial r^2} \tag{2.5}$$

$$(c_e)_{r=R_n} = 0 \qquad (c_e)_{r=R_n+\delta_{sei(t)}} = ce \tag{2.6}$$

2.2.3 *Mixed Solvent Diffusion and Solvent-Reduction Kinetics Models*

2.2.3.1 Safari's Model

In Safari et al.'s model[5], they presented a model which includes both kinetic limitation and diffusion limitation. The solvent-reduction kinetic follows Tafel's equation which is similar to Ramadass's work, while they neglected the equilibrium potential in the exponential term to reduce the total number of adjustable parameters

$$i_{sei} = -a_n l_n F k_{sei} c_{e,0} e^{-\frac{\alpha_c F}{RT}(\phi_n - \frac{i_{app} R_{sei}}{anln})} \tag{2.7}$$

where $c_{e,0}$ is the solvent concentration at the graphite-SEI layer interface.

The transport of solvent molecules through the SEI layer form is derived from the overall material balance. Since the length is much smaller compared to the active-material particle size, the SEI layer is simplified with a planar geometry. Both diffusion and convection terms are included in the transport limitation

$$\frac{\partial c_e}{\partial t} = D_{sei} \frac{\partial^2 c_{sei}}{\partial r^2} - v \frac{\partial c_e}{\partial r} \tag{2.8}$$

$$v = \frac{d\delta}{dt} \tag{2.9}$$

$$\left(-D_{sei} \frac{\partial c_e}{\partial r} + v c_e\right)_{r=R_n} = \frac{i_{sei}}{a_n l_n F} \qquad (c_e)_{r=R_n+\delta_{Sei}} = \ c_{e0} * \epsilon_{sei} \tag{2.10}$$

where v is the SEI layer velocity, ϵ_{sei} is the SEI layer porosity.

The expression for SEI layer growth rate is not exactly same with Ramadass's model. This model has a coefficient two in denominator.

$$\frac{\partial \delta_{sei}}{\partial t} = -\frac{i_{sei} M_{sei}}{2 \cdot a_n l_n F \rho_{sei}} \tag{2.11}$$

Their model considers both solvent decomposition kinetics and solvent diffusion through the SEI film. However, they simulated diffusion-limited case and kinetic-limited case separately instead of using the mixed model they proposed.

2.2.3.2 Ekstrom's Model

Ekstrom's[8] model combines the cathodic Tafel equation of solvent reduction current expression and the linear solvent diffusion through the SEI layer. There is no resistance term in their Tafel equation. Even in their model, the SEI film morphology is not uniform and consist of micropores and macropores layer, however, the kinetic expressions for both micropores and macropores are the same. The current density from the SEI parasitic reaction is the parallel current of the kinetic-limited current density and the diffusion-limited current density

$$i_{sei,kin_m} = -\epsilon_m a_n l_n i0_{sei} e^{-\frac{\alpha_c F}{RT}(\phi_n - U_{sei})} \quad m = mic, mac \tag{2.12}$$

$$i_{sei,lim_m} = -\frac{\epsilon_m ce D_m F a_n l_n}{s} \quad m = mic, mac \tag{2.13}$$

$$i_{sei_m} = \frac{i_{sei,kin_m}}{1+\frac{i_{sei,kin_m}}{i_{sei,lim_m}}} \tag{2.14}$$

where i_{sei,kin_m} is the kinetic limiting current, i_{sei,lim_m} is the diffusion limiting current, ϵ_m is the volume fraction of the micropores layer or the macropores layer, $i0_{sei}$ is the exchange current density.

2.2.3.3 Lin's Model

Lin et al.[4] present another approximation to combine both the kinetic limitation and diffusion limitation. An SEI layer thickness dependent limiting factor is introduced to simplify the solvent diffusion limitation

$$R(\delta_{sei}) \approx e^{-\lambda \delta_{sei}} \tag{2.15}$$

where $R(\delta_{sei})$ is the limiting factor and ranges from 0 to 1. λ is the limiting coefficient.

After applying the limiting factor to the Tafel's equation, the final current density equation for SEI layer parasitic reaction is shown below.

$$i_{sei} = a_n l_n e^{-\lambda \delta_{sei}} F k_{sei} ce \cdot e^{-\frac{\alpha_c F}{RT}(\phi_n)} \tag{2.16}$$

2.3 SEI LAYER MORPHOLOGY

A majority of SEI film formation models suppose that the SEI layer is a single uniform phase. Ekstrom's[8] contribution in this topic is that their SEI parasitic reaction model includes a stable micropores SEI layer and a macropores SEI layer formed from crack due to graphite expansion. The overall current density from the SEI layer is the linear combination of the micropores and macropores current densities as Eq.2.17.

$$i_{sei} = i_{sei_{mic}} + i_{sei_{mac}} \tag{2.17}$$

The different terms to distinguish $i_{sei_{mic}}$ and $i_{sei_{mac}}$ are ϵ_m and D_m. The ϵ_{mic} is constant while ϵ_{mac} is related to the stoichiometric coefficient for lithium in Li_xC_6 which is assumed to be proportional to a piecewise expansion factor. The diffusion coefficients of two different layers depend on the tortuosity that was taken as equal in their model.

Chapter 3. NUMERICAL INPLEMENTATION

To predict the Lithium-ion battery cycling life performance, as mentioned before, plenty of models have been proposed. In this work, we generally focus on SPM which consists of two partial differential governing equations (PDEs), two Bulter-Volmer equations and several additional algebraic equations listed in previous section. Combined with the SEI parasitic models discussed in the previous chapter, those models have different PDEs sets. In this chapter, we applied first principle kinetic limited model, Ploehn's diffusions limited model and Safari's mixed model separately to SP model separately. Finite Difference (FD) method is first used to discretize the solid phase concentration along with r-direction and convert all partial differential equations to Ordinary Differential Equations (ODEs). After that, ODEs are solved in time using the numerical method of lines approaches.

In this chapter, we mainly study how those mechanisms affect the numerical implementation. Based on those methods, the minimum node point for FD method and the maximum time step size for Euler backward and Euler forward are first studied for three SEI layer models. The stability of the numerical methods is test by comparing the maximum time step.

3.1 FINITE DIFFERENCE METHOD

3.1.1 *Finite Difference Method*

Finite Difference Method is a numerical method for solving differential equations by approximate the derivatives using finite differences. It is a common approach to numerically solve the partial differential equations.

In this case, the solid phase concentration $c_{s,i}$ is discretized along with the r-axis by N+2 node points. As a result, the step size h is $\frac{R_i}{1+N}$. The N is the number of nodes and R_i is the radius of particles. More node points result in more equations which increases the accuracy.

The approximation for $r = 0$ which is at $i = 0$ listed below.

$$\frac{dc_0}{dr} = \frac{1}{2} \cdot \frac{-c_2 - 3 \cdot c_0 + 4 \cdot c_1}{h} \; at \; r = 0 \tag{3.1}$$

For boundary condition at $r = R_i$, the approximation form is same as $r = 0$.

$$\frac{dc_{N+1}}{dr} = \frac{1}{2} \cdot \frac{c_{N-1} + 3 \cdot c_{N+1} - 4 \cdot c_N}{h} at \; r = R_i \tag{3.2}$$

For other node points along the r-axis, they follow the equations listed below.

$$\frac{dc_i}{dr} = \frac{1}{2} \cdot \frac{c_{i+1} - c_{i-1}}{h} \; for \; i = 1 \; to \; N \tag{3.3}$$

$$\frac{d^2c_i}{dr^2} = \frac{1}{2} \cdot \frac{c_{i-1} - 2c_i + c_{i+1}}{h^2} \; for \; i = 1 \; to \; N \tag{3.4}$$

After applying those derivatives approximation, the PDEs are transformed into DAEs set which could be solved using Maple *dsolve* package or numerical method of lines approaches.

3.1.2 *Finite Difference Convergence*

From the last section, we know that more node point gives better accuracy. To find the minimum node point needed, the FD method and the *dsolve* package are utilized to solve the original PDEs and find out the minimum node points for convergence of the three different SEI formation models.

The kinetic model includes only two PDEs. Node points from 1 to 7 for two electrodes are compared by solving the equation set and plotting the discharge and charge of the first cycle at 1C CCCV charging rate.

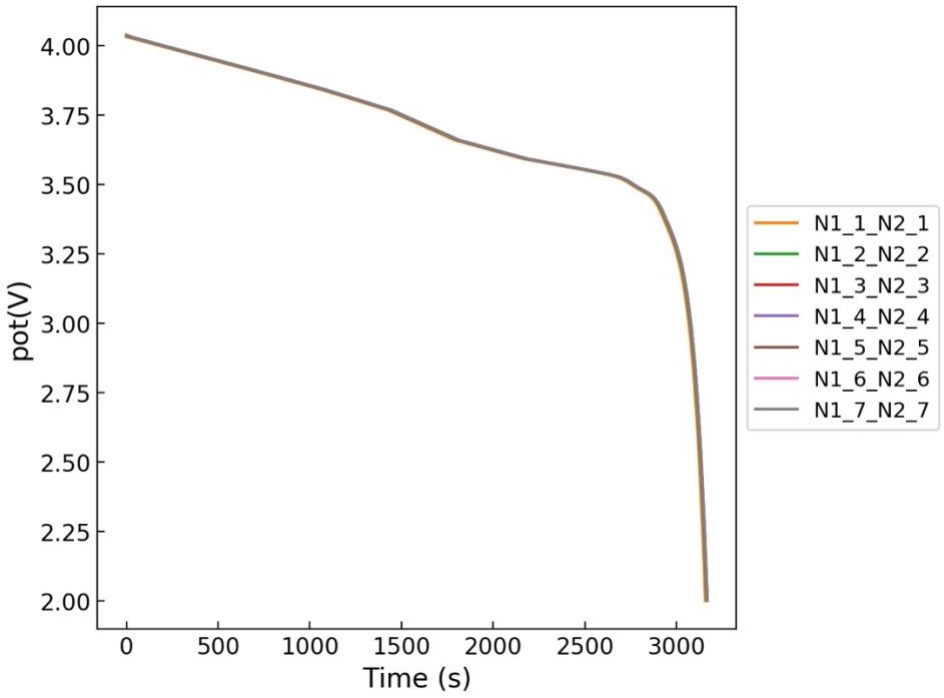

Figure 3.1. First discharge potential change with time of kinetic limited model

Figure 3.1 shows the discharge voltage change with time plot. There is no significant difference with increasing node points.

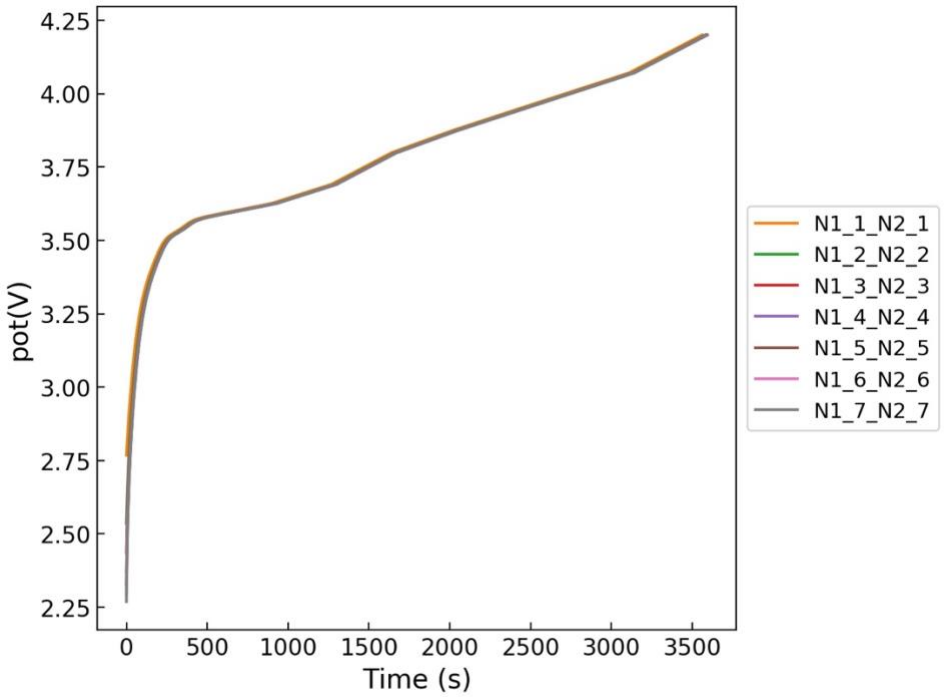

Figure 3.2. First charge potential change with time of kinetic limited model

Figure 3.2 shows the voltage curve of the first charge cycle. The voltage curves converge at five node points for each electrode.

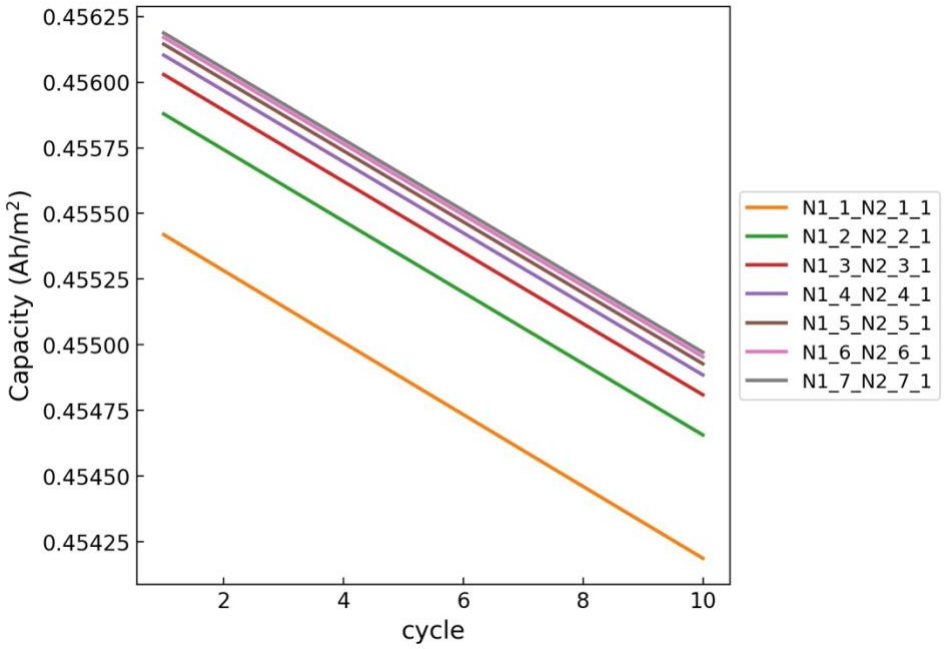

Figure 3.3. Discharge capacity change with cycles of kinetic limited model

From the first cycle's variable plots, five nodes points are enough for r-axis finite difference method. To make sure it also accurate for cycling simulation, we simulated the model for cycling process as well. Figure 3.3 shows that it converges at six node points. In short, after those comparisons, six node points are needed for finite difference method for the kinetic limited model.

Next, the diffusion limited model is checked. In diffusion limited model, besides two diffusion partial differential equations through electrodes, it also involves another transport partial differential equation through the SEI layer. The node point needed for the SEI layer should be tested further.

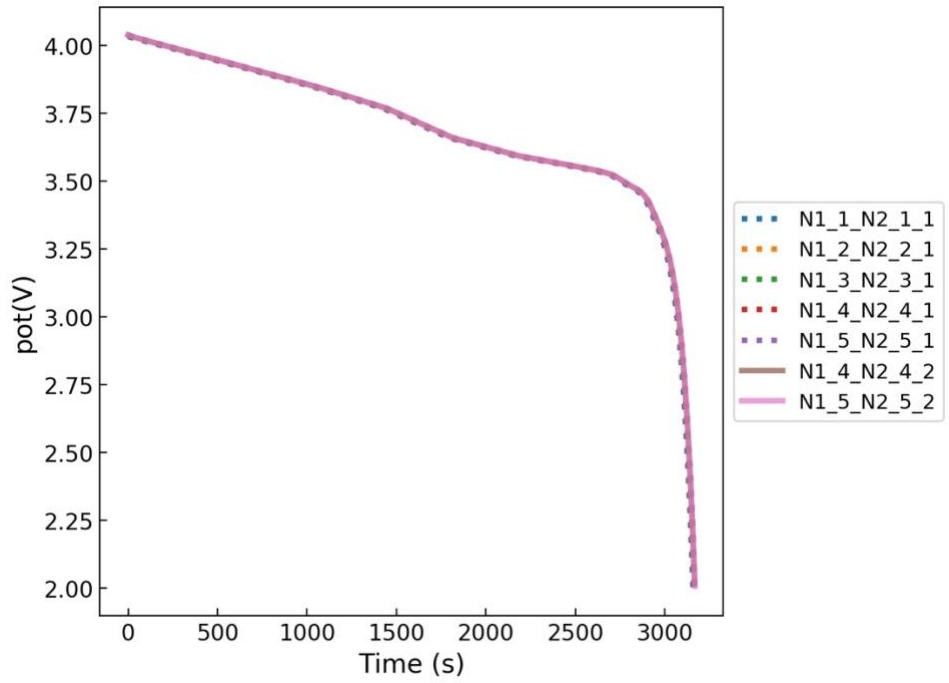

Figure 3.4. First discharge potential change with time of diffusion limited model

According to Figure 3.4, the increasing node points has no noticeable effect on first cycle discharge capacity.

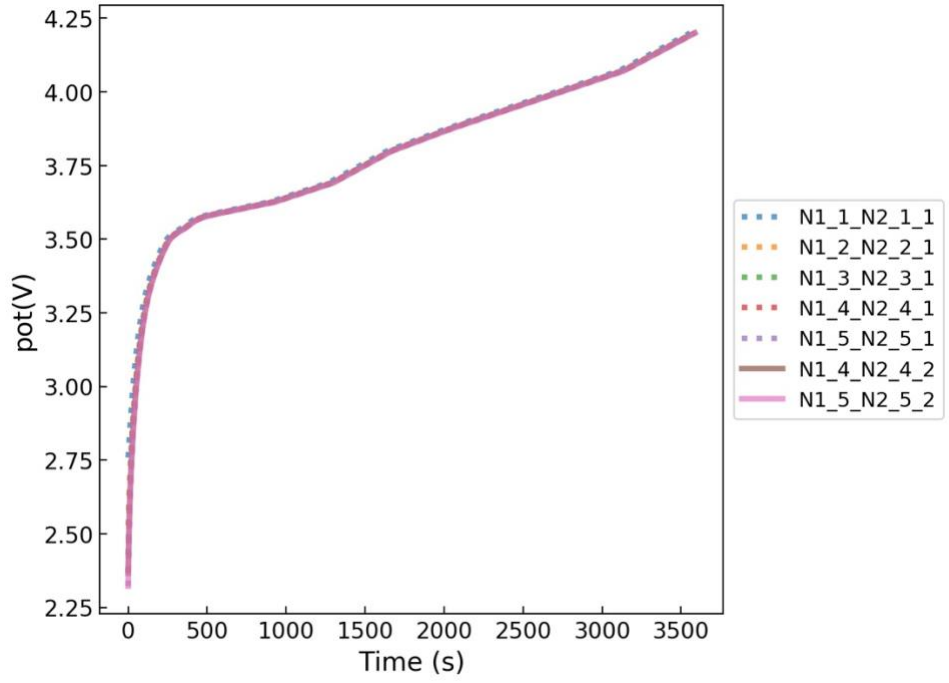

Figure 3.5. First charge potential change with time of diffusion limited model

Figure 3.5 gives the potential change with time during the first charge process. It will be more evident to zoom in from 0 seconds to 150 seconds.

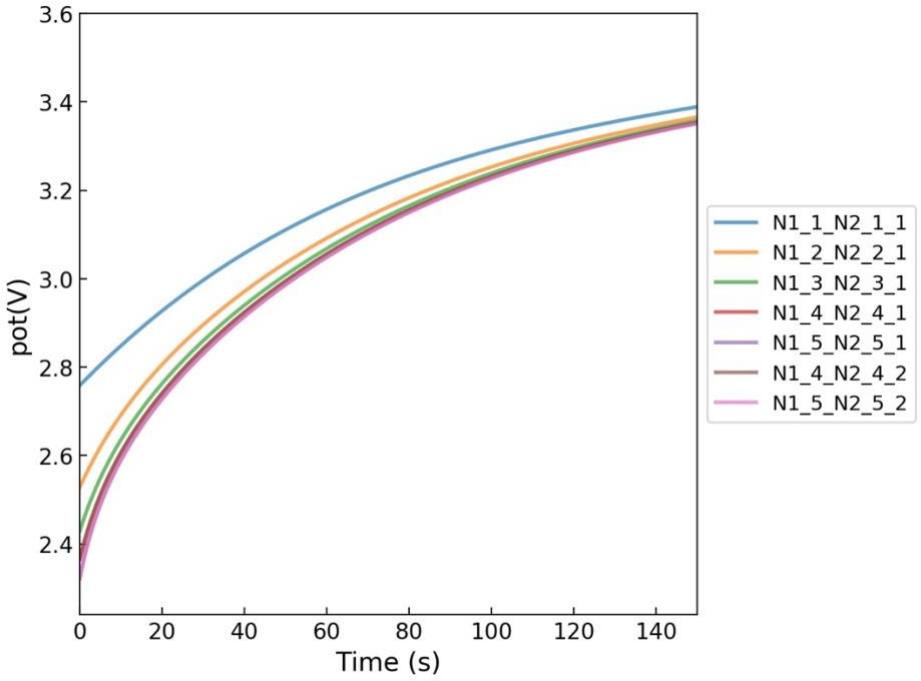

Figure 3.6. First charge potential change with time of diffusion limited model

The Figure 3.6 displays that for diffusion limited model, five node points for electrodes and one point for SEI layer can converge the curves.

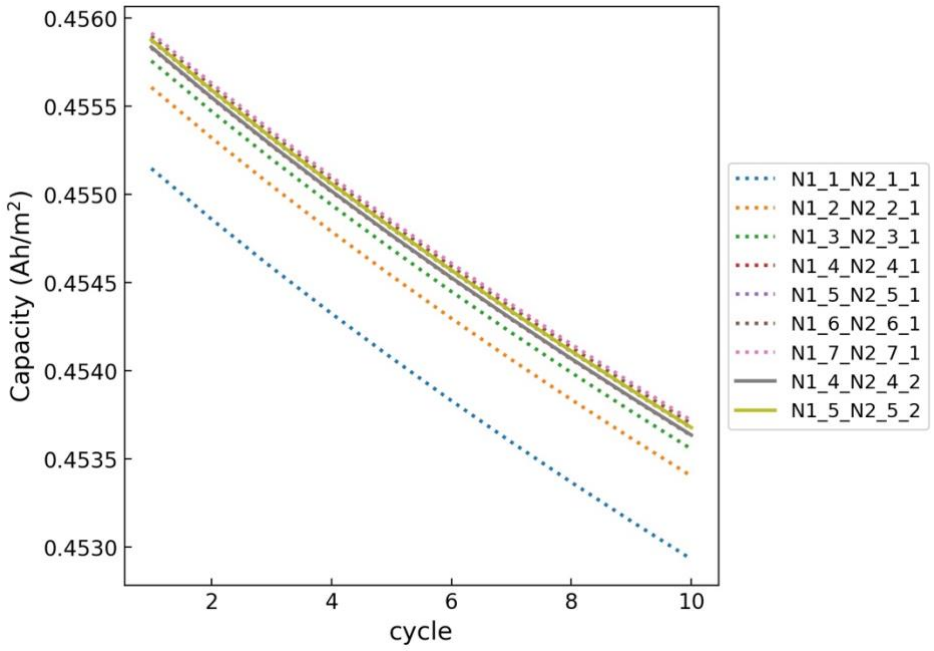

Figure 3.7. Discharge capacity change with cycles of diffusion limited model

Based on discharge capacity change with cycles comparison and the first charge potential results, five node points for electrodes and one node point for SEI layer should be used.

Last, mixed kinetic and diffusion limited model is studied. Similar to diffusion limited model, it has three partial differential equations. Three node points number should be checked.

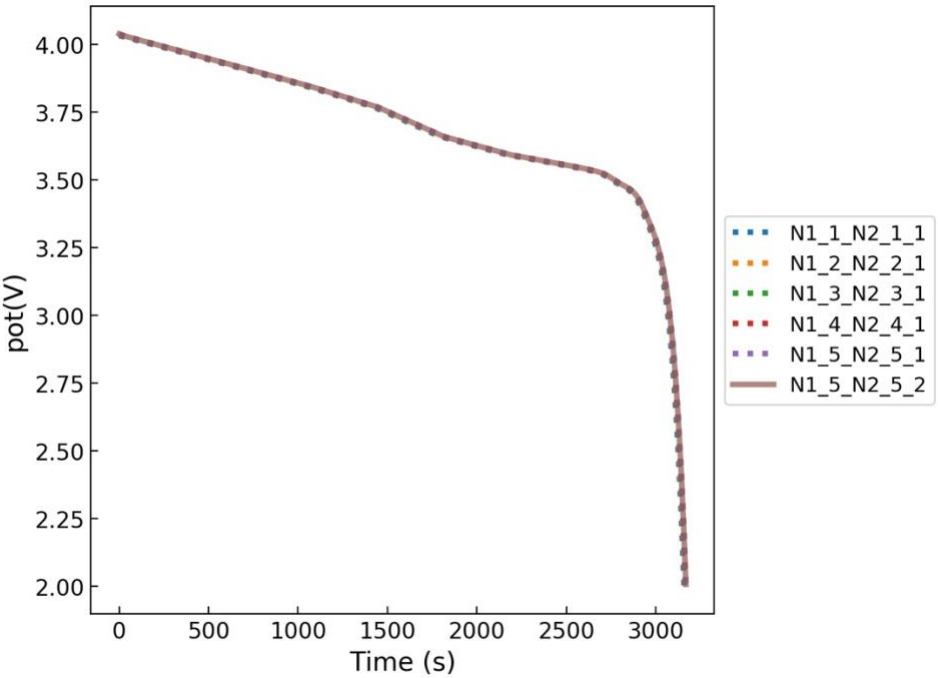

Figure 3.8. First discharge potential change with time of mixed model

Figure 3.8 tells that different node points don't affect first discharge potential.

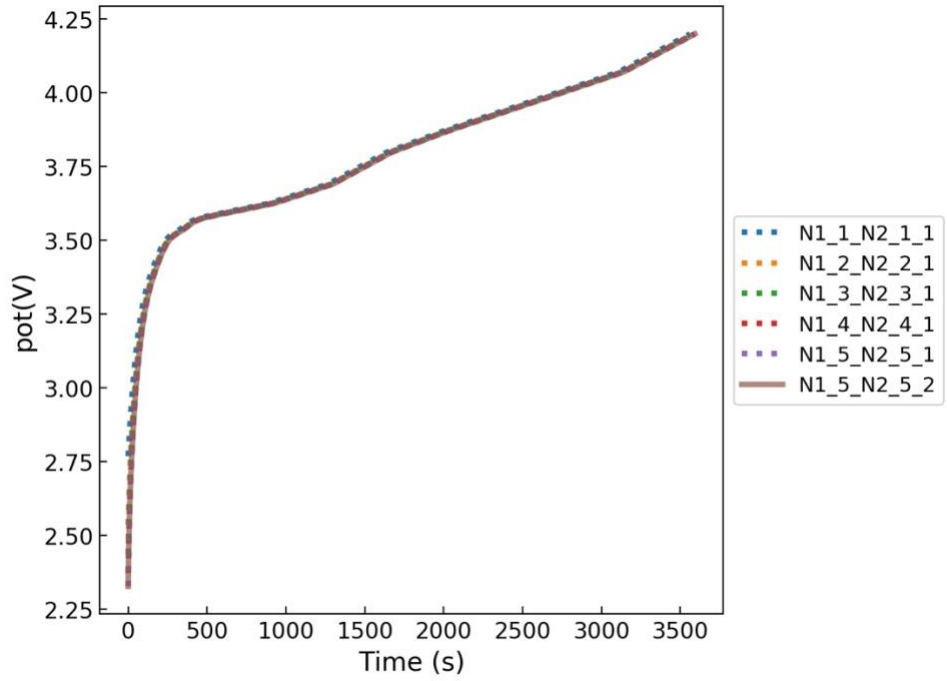

Figure 3.9. First charge potential change with time of mixed limited model

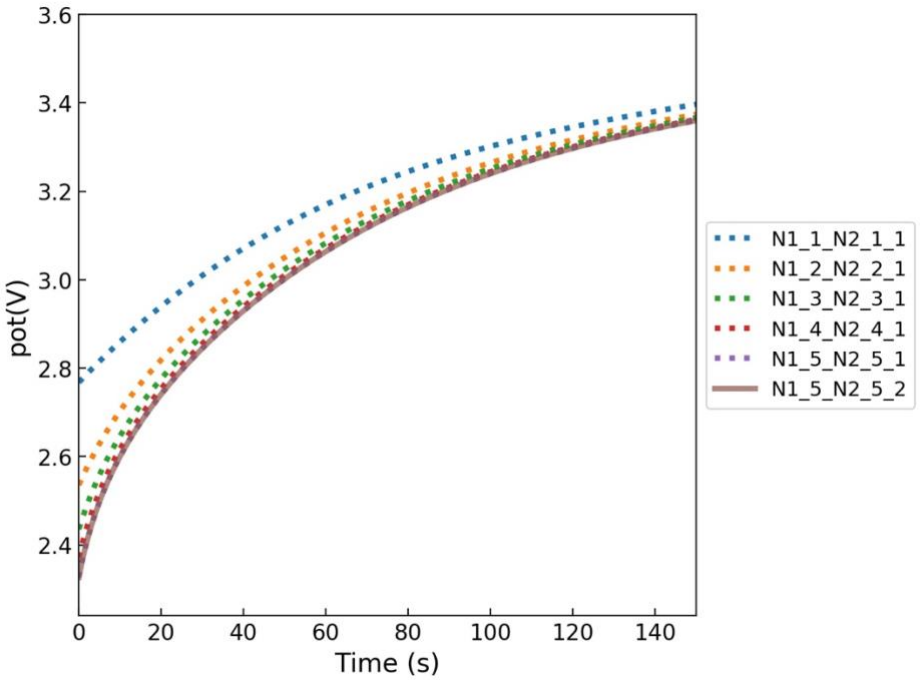

Figure 3.10. First charge potential change with time of mixed model

Figure 3.10 shows five node points for two electrodes and one node points for SEI layer are appropriate.

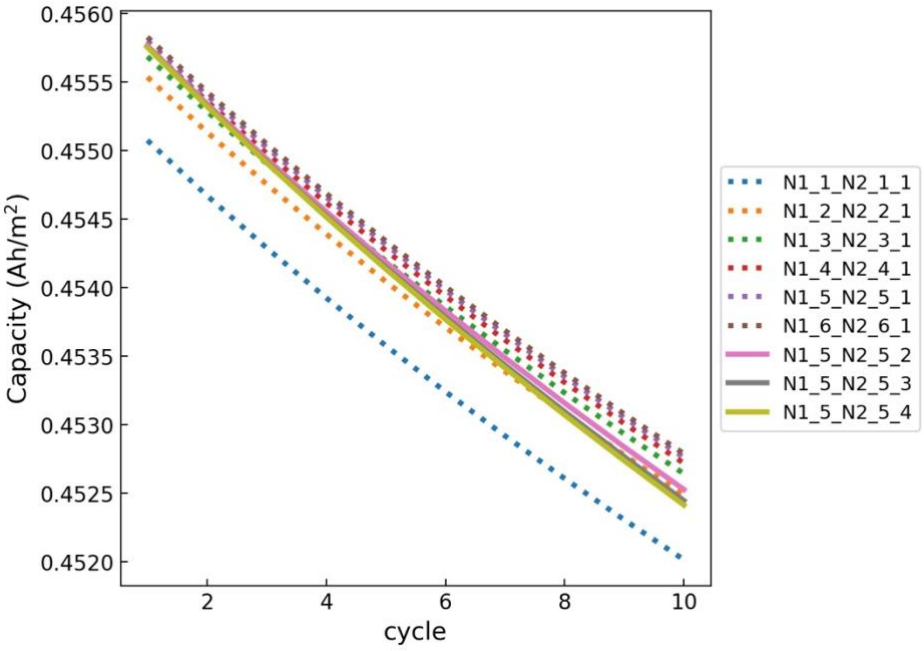

Figure 3.11. Discharge capacity change with cycles of mixed model

From Figure 3.11, two node point through the SEI layer is not enough for the mixed model; three node point is more accurate. To sum up, five node point for electrodes and three node point for SEI layer are reasonable for mixed model as shown in Table 3.1.

Table 3.1. Minimum node point needed

	Kinetic limited	Diffusion limited	Mixed model
N1(anode)	6	6	5
N2 (cathode)	6	6	5
N3 (SEI layer)	-	1	3

3.2 Euler Forward and Euler Backward Methods

3.2.1 *Euler Backward and Euler Forward*

Euler method is the most basic numerical method for solving ordinary differential equations with a given initial value. It is a first-order numerical procedure. It also called Euler forward method or explicit method. Euler backward method is another primary numerical method for the solutions of ODEs which in contrast is an implicit method. The main idea of Euler methods is to solve the

ODEs time step by time step from the starting point. Take h as the small-time step and assume the slope does not change too much along this small-time step.

Both Euler forward and backward methods can be derivative from Taylor series. Let's start with the Euler forward

$$Y0 = y(t) \tag{3.5}$$

$$Y1 = y(t + h) \tag{3.6}$$

Convert the right-hand side of $Y1$ equation as a series in h and get the first order accuracy

$$Y1 = y(t) + D(y)(t) \cdot h = Y0 + F0 \cdot h \tag{3.7}$$

where $F0$ is the derivative at time equal to t.

For Euler backward, it also starts with $Y0$ and $Y1$. However, it looks back to previous time step instead of forward step

$$Y0 = y(t - h) \tag{3.8}$$

$$Y1 = y(t) \tag{3.9}$$

Convert the right-hand side of $Y0$ equation as a series in h and get the second order accuracy

$$Y0 = y(t) - D(y)(t) \cdot h = Y1 - F1 \cdot h \tag{3.10}$$

$$Y1 = Y0 + F1 \cdot h \tag{3.11}$$

where $F1$ is the derivative at time equal to $t + h$.

After applied Euler forward or backward approaches to the next time step, the DAEs become a set of algebraic equations at this step. Next, Newton Raphson Method is used to solve this nonlinear equation set. Then all solution at this time step can be obtained. Repeat this process, the DAEs can numerically solved at a certain time step.

3.2.2 *Numerical Methods Stability*

Numerical stability is an essential property of numerical methods. A test equation is used to analyze the stability of the numerical algorithms.

$$\frac{dy}{dt} = ky,\ y(0) = 1\ with\ k\ \in \mathbb{C} \tag{3.12}$$

The analytical solution of the test equation is $y = e^{kt}$, which approaches zero as $t \to \infty$ when $Re(k) < 0$. If the numerical method exhibits this behavior (for a fixed time step), it is an A-stable

method. When depicted on the complex plane, the entire negative plane is available for A-stable methods. Figure 3.12 is the Euler forward stability region.

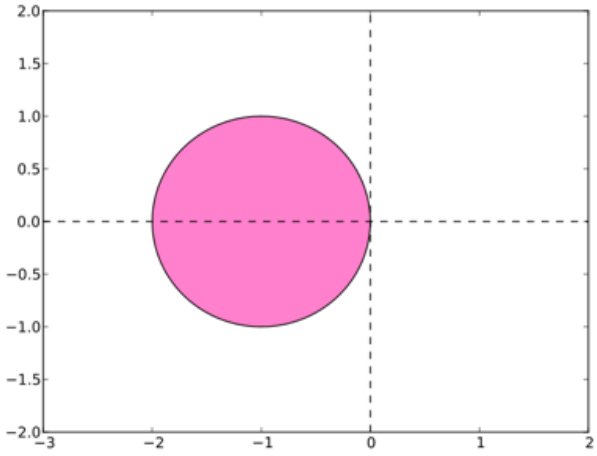

Figure 3.12. Euler Forward stability region[20]

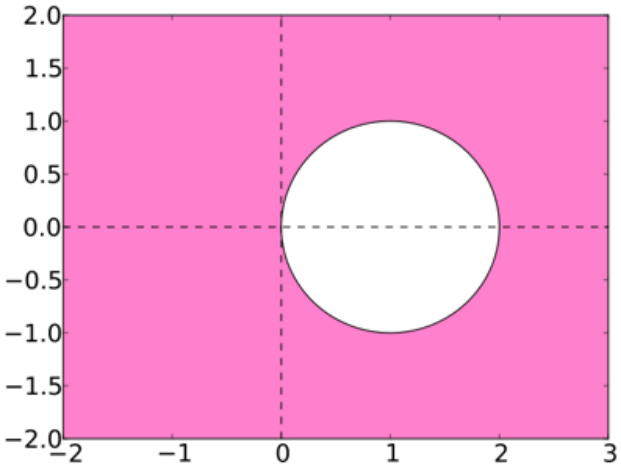

Figure 3.13. Euler Backward stability region[20]

Euler Backward is an A-stable method as shown in Figure 3.13 which has the whole negative plane available for test equation while Euler Forward has a more limited region.

Different mechanisms will obviously affect the stability of those numerical methods. In this section, the effects of those mechanisms are tested. Since the SEI growth is assumed to happen during the charging process, the maximum time step of three mechanisms must be same for discharge process. However, the charging process will show the stability-diversity of those

chemical limitations. Different charging rate is also applied to compare the influence of stability. The results are summarized in the table below.

Table 3.2 is the Euler Forward stability.

Table 3.2. Euler Forward stability

Charge Rate	Discharge	Charge		
		Kinetic limited model	Diffusion limited model	Mixed model
1C	3.1	3	3	3
0.5C	3.1	3	3	3
0.1C	3.1	3	3	3

From the Figure 3.2, the maximum time steps for three mechanism models are same even for different charging rate. According with the complex plane results, practical time step for Euler Forward is insufficient.

Table 3.3 shows the Euler Backward stability.

Table 3.3. Euler Backward stability

Charge Rate	Discharge	Charge		
		Kinetic limited model	Diffusion limited model	Mixed model
1C	59	87	939	85
0.5C	105	207	1894	200
0.1C	529	1358	9563	1312

According to the table, lower discharge/charge rate give a broad range time step selectivity which conforms to reality. The process time of 0.1C discharge/charge rate is about ten times to 1C discharge/charge rate which corresponds to the result that the maximum time step is also around ten times. That means the charge/discharge rate doesn’t have a noticeable impact on numerical method’s stability.

When focus on the influence of mechanisms, it is evident that the diffusion limited model is more stable in term of the maximum time step. The diffusion limited model is actually a moving boundary problem while it is more stable compared to kinetic limited model based on SPM. kinetic equation decides the mixed model’s effect on method stability since their maximum time step is close to kinetic limited model. In most cycling battery P2D model, a kinetic limited model is used to describe the SEI layer growth. In our future work, we will apply the diffusion limited mechanism

and the mixed mechanism to P2D model. It may help decrease the solving time and increase the stability of the whole system.

Chapter 4. SIMULATION AND RESULTS

4.1 SIMULATION PROCESS

In this study, three different mechanisms are tested for three different charge rates. The three mechanisms are the first principle kinetic limited model, the dilute theory diffusion limited model and the safari's mixed model. The three rates are 1C, 0.5C and 0.1C and the discharge rate is 0.5C. The cycling process follows a conventional constant current discharge, constant current (CC) charge and constant voltage (CV) charge protocol. The CC charge stop condition is the potential equal to 4.2V and the discharge stop potential is 2V.

4.2 RESULTS

Firstly, the capacity fade after 400 cycles is tested for three mechanisms. The results for 1C charge and 0.5C charge are listed below Figure 4.1and Figure 4.2

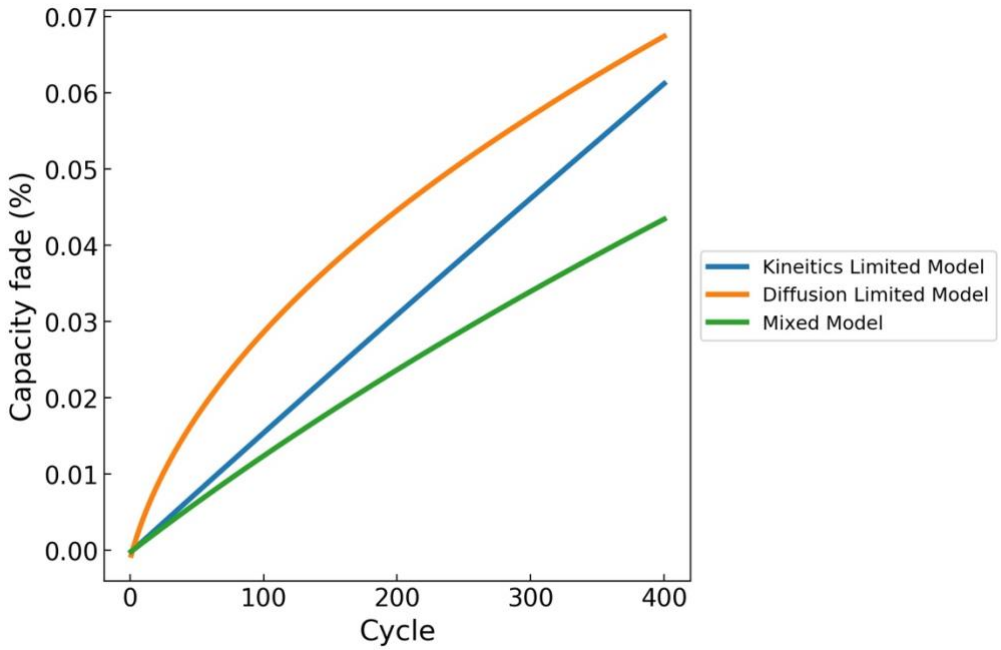

Figure 4.1. 1C charge capacity fade of three SEI layer models

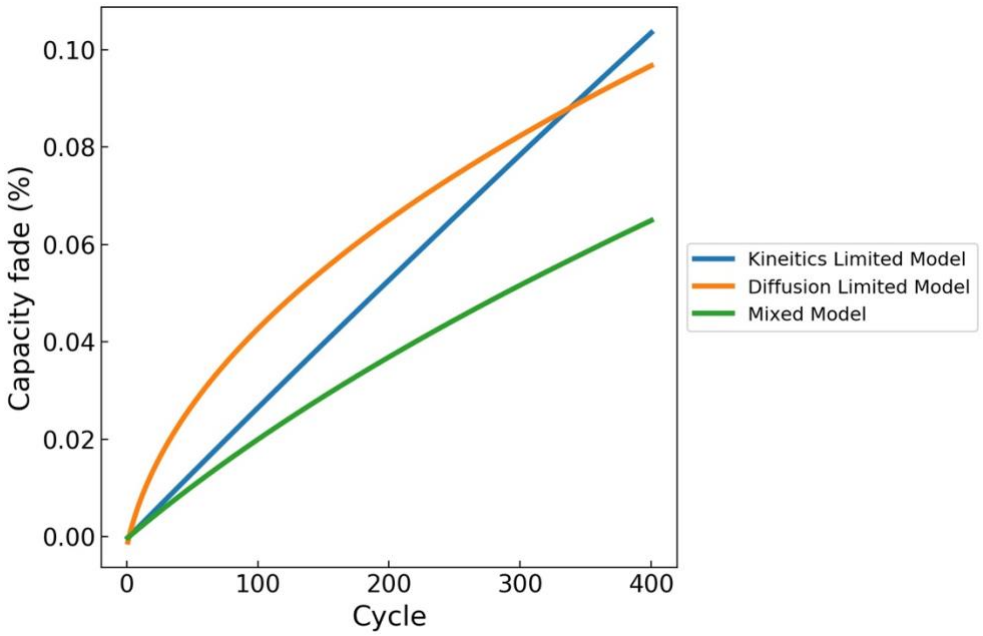

Figure 4.2. 0.5C charge capacity fade of three SEI layer models

It's predictable that the mixed model, with more limitation for SEI growth, has a lower capacity fade after 400 cycles in comparison to other two models. The kinetics model shows a linear capacity fade increasing trend while the diffusion gives a quadratic trend. The mixed model's trend is the combination of kinetic limited model and diffusion limited model.

Next, charging rate study has been applied to both kinetic limited and diffusion limited mechanisms.

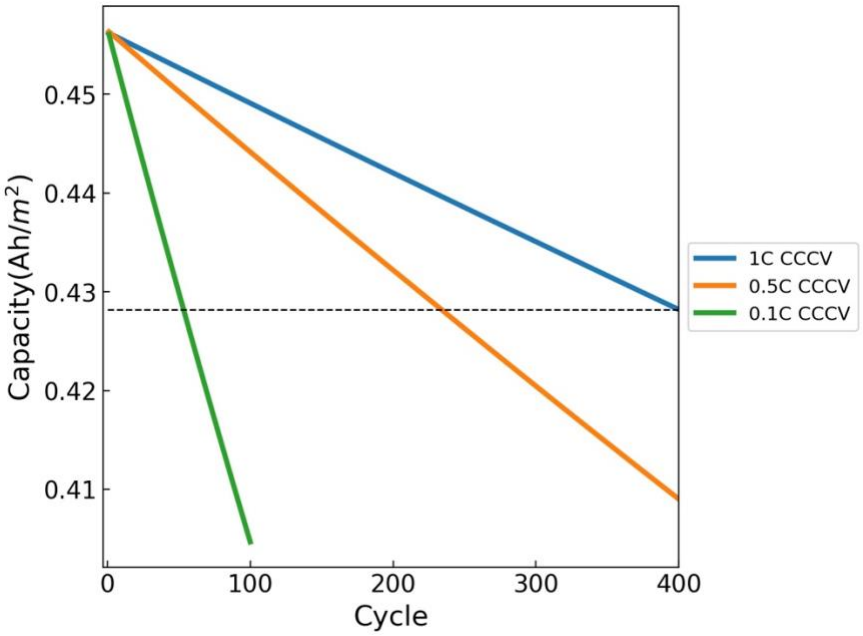

Figure 4.3. Kinetic limited model capacity degradation for different charge rate

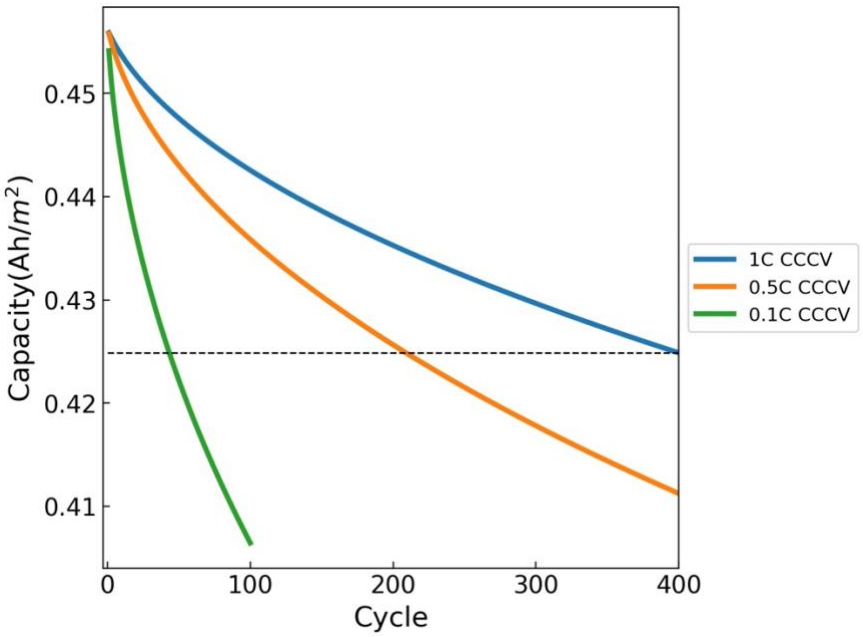

Figure 4.4. Transport limited model capacity degradation for different charge rate

Both Figure 4.3 and Figure 4.4 demonstrate that lower charging rate leads to higher capacity fade. This result may due to the long charge time of lower charge rate. Based on the experience on the capacity fade study, this phenomenon is not unique for this certain battery. However, some other batteries may have an opposite trend. The capacity fade after 400 cycles is 6.8% of diffusion

limited model and 6.14% of kinetic limited model. For mixed model, the capacity fade after 400 cycles is 4.34% as shown in Figure 4.5.

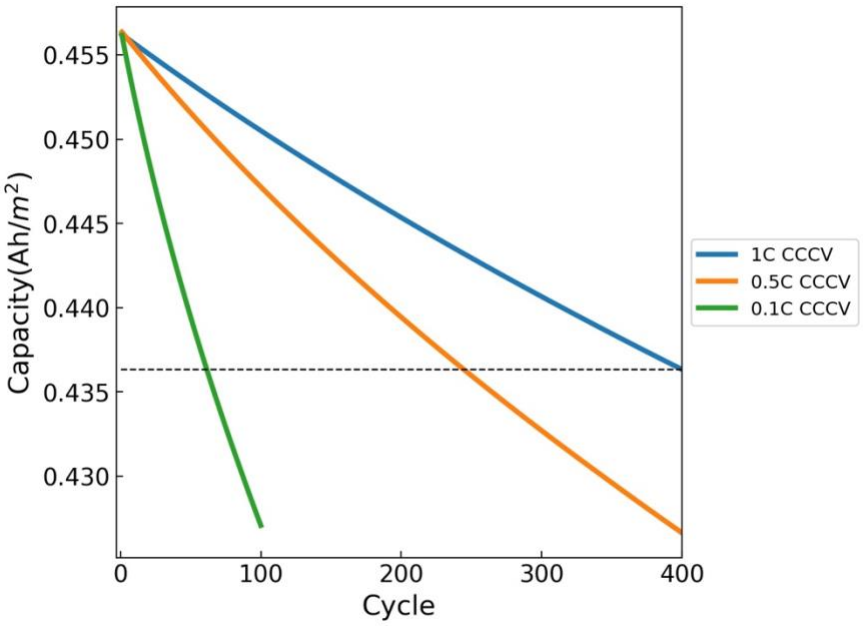

Figure 4.5. Mix model capacity degradation for different charge rate

To compare that how different charging rates affect the mechanisms, all 4.34% capacity fade cycle number are listed in the Table 4.1 for three models and three charge rates.

Table 4.1. 4.34% Capacity fade cycle number

Charge Rate	1CCCV	0.5CCCV	0.1CCCV
Kinetic limited	282	165	38
Diffusion limited	188	99	21
Mixed model	400	245	61

From the Table 4.2, the Mixed model has the highest cycle difference which means it is more sensitive to changing rate.

Table 4.2. Capacity fade cycle number difference

	Δcycle (1C to 0.5C)	**Δcycle** (1C TO 0.5C)
Kinetic limited	282	165
Diffusion limited	188	99
Mixed model	400	245

The side reaction current density changing with time during charge process is studied for three mechanisms. This study helps to explore the impact of those mechanisms on the SEI formation.

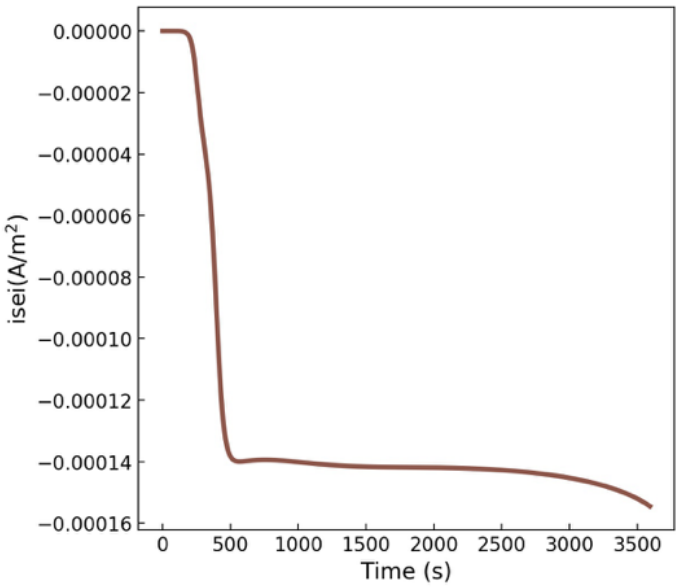

Figure 4.6. SEI side reaction current density of kinetic limited model

Figure 4.6 indicates that the SEI formation rate increases rapidly within 500s and remain unchanged for next 2500s for the kinetic limited model.

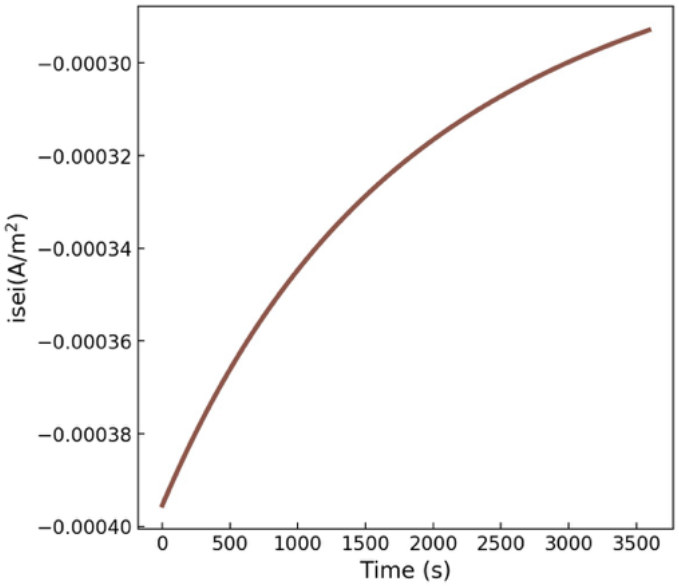

Figure 4.7. SEI side reaction current density of transport limited model

In Figure 4.7, the continually decrease curve informs that the SEI side reaction rate keeps decline during the charge process for the diffusion limited model.

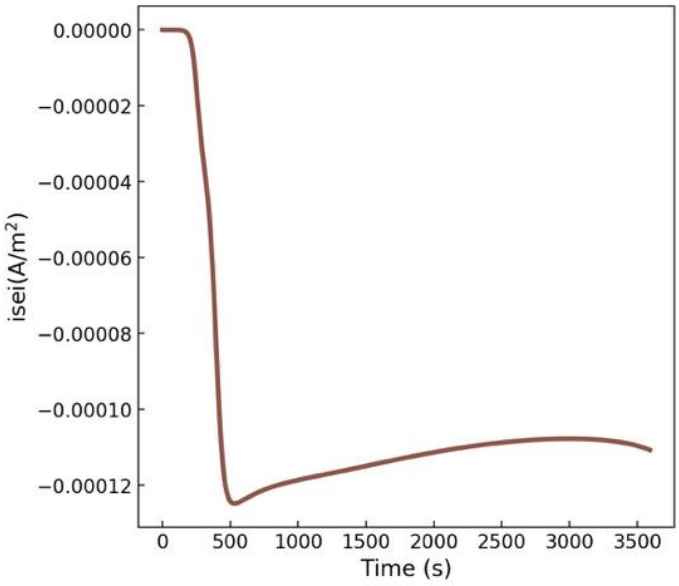

Figure 4.8. SEI side reaction current density of mixed limited model

The SEI formation rate of the mixed limited model is exhibited in Figure 4.8. The trend of the mixed model is like the combination of kinetic limited model and diffusion limited model which has a mushrooming trend in the first 500s and a relatively flat decreasing trend after 500s. This result obeys the physical phenomenon. At the beginning of each charge operation, the SEI film thickness is the thinnest which give the less limitation for solvent transportation. Along with the SEI layer growth, the solvent concertation at graphite and SEI film interface is decreasing. As a result, the reaction rate starts decreases.

4.3 CONCLUSION

Capacity degradation study is a critical topic for battery performance simulation. It is impending to develop a comprehensive and precise SEI film formation model. A better understanding of the SEI film formation process will help to decrease the capacity fade and also assist with parameter estimation.

In this study, several recent reported physics-based SEI layer models are first reviewed. Then, the numerical implementation is studied depend on three mechanisms. Finite difference method is applied to discretize the r direction. The minimum node points for the single particle model are investigated for each mechanism. After that, a stability analysis is used to probe the effect of different mechanisms on numerical methods. The transport-only limited model is the most stable model even it's a moving boundary problem. Finally, the cycling life study indicates that capacity

fade and charge rate have an inverse ratio relationship. The SEI side reaction rate curve demonstrates that the side reaction starts with the kinetic limitation and following the diffusion limitation. There is no apparent reason to ignore any constraint. Even the mixed model used in this study was reported in 2009 by Safari et.al., they didn't use this model to simulate the battery capacity fade. This study is the first attempt to apply this full mixed model.

BIBLIOGRAPHY

[1] P. Arora, R. E. White, M. Doyle, J. Electrochem. Soc., 145, 3647-3667 (1998).

[2] J. Park, J. H. Seo, G. Plett, W. Lu, A. M. Sastry, Electrochem. Solid-State Lett., 14, A14 (2011).

[3] Y. Dai, L. Cai, R. E. White, J. Electrochem. Soc., 160, A182 (2013).

[4] X. Lin, J. Park, L. Liu, Y. Lee, A. M. Sastry, J. Electrochem. Soc., 160 (10) A1701-A1710 (2013).

[5] M. Safari, M. Morcrette, A. Teyssot, and C. Delacourt, J. Electrochem. Soc., 156(3), A145-A153 (2009).

[6] P. Ramadass, B. S. Haran, P. M. Gomadam, R. H. White, and B. N. Popov, J. Electrochem. Soc., 151, A196 (2004).

[7] M. B. Pinson, M. Z. Bazant, J. Electrochem. Soc., 160 (2) A243-A250 (2013).

[8] H. Ekström, G. Lindbergh, J. Electrochem. Soc., 162 (6) A1003-A1007 (2015).

[9] C. Y. Wang, W. B. Gu, and B. Y. Liaw, J. Electrochem. Soc., 145, 3407 (1998).

[10] W. B. Gu, C. Y. Wang, and B. Y. Liaw, J. Electrochem. Soc., 145, 3418 (1998).

[11] P. W. C. Northrop, V. Ramadesigan, S. De and V. R. Subramanian, J. Electrochem. Soc., 158 (12) A1461-A1477 (2011).

[12] V. Boovaragavan, V. Ramadesigan, and V. R. Subramanian, J. Electrochem. Soc., 157 (7) A854-A860 (2010).

[13] R. Allen, ElectronicDesign 3/26,26(2010).

[14] M. T. Lawder, P. W. C. Northrop and V. R. Subramanian, J. Electrochem. Soc., 161 (14) A2099-A2018 (2014).

[15] P. Keil, S. F. Schuster, J. Wilhelm, J. Travi, A. Hause, R. C. Karl and A. Jossen, J. Electrochem. Soc., 163 (9) A1872-A1880 (2016).

[16] S. Atlung, K. West, and T. Jacobsen, J. Electrochem. Soc., 126, 1311 (1979).

[17] S. J. Moura, N. A. Chaturvedi and M. Krstic, J. Dyn. Sys., Meas., Control 136 (1), 011015(2013).

[18] R. Darling, J. Newman, J. Electrochem. Soc. 145, 990 (1998).

[19] H. J. Ploehn, P. Ramadass and R. E. White, J. Electrochem. Soc., 151 (3) A456-A462 (2004).

[20] https://en.wikipedia.org/wiki/Euler_method

APPENDIX A

Table A.3. List of variables for Li-ion battery model

Symbol	Variables
$c_{s,i}$	Solid phase lithium concentration, $\mathrm{mol/m^3}$
c_{s,R_i}	Solid phase lithium concentration at electrode surface, $\mathrm{mol/m^3}$
U_i	Open circuit potential vs Li electrode, V
$i_{int,i}$	Intercalation current density referred to interfacial surface area of anode, $\mathrm{A/m^2}$
i_{app}	Applied current density, $\mathrm{A/m^2}$
j_i	Pore wall flux associated with normal intercalation, $\mathrm{mol/m^2 s}$
i_{sei}	SEI side reaction current density referred to interfacial surface area of anode, $\mathrm{A/m^2}$
ϕ_i	Solid phase potential, V
δ_{sei}	SEI layer thickness, m

Table A.4. Parameters used in the mathematical model

Symbol	Unit	Description	Value	
			Anode	**Cathode**
$D_{s,i}$	m^2/s	Solid phase diffusion coefficient	$2{\cdot}10^{-14}$	$1{\cdot}10^{-14}$
$c_{i,max}$	mol/m^3	Maximum solid phase concentration	30555	51555
a_i	m^2/m^3	particle surface area to volume	11364	12500
l_i	m	length of the electrode	$88{\cdot}10^{-6}$	$80{\cdot}10^{-6}$
R_i	μm	Active particles radius	2	2
k_i	m/s	Rate constant for lithium intercalation reaction	$1.4{\cdot}10^{-9}$	$7{\cdot}10^{-10}$
$SOC_{i,0}$	-	Initial state of charge	0.74	0.5
R	$J/(mol{\cdot}K)$	Gas constant	8.3143	
T	K	Temperature	298.15	
F	C/mol	Faraday's constant	96487	
			Anode SEI parameters	
ce	mol/m^3	Electrolyte concentration	4541	
M_{sei}	kg/mol	Molecular weight of SEI	0.162	
ρ_{sei}	kg/m^3	SEI density	1690	
κ_{sei}	S/m	SEI ionic conductivity	$5{\cdot}10^{-6}$	
k_{sei}	m/s	Rate constant of side reaction	$2.4{\cdot}10^{-12}$	
D_{sei}	m^2/s	SEI film diffusion coefficient	$6.8{\cdot}10^{-21}$	
$R_{s,0}$	m^2/S	Initial SEI resistance	0.001	
$\delta_{sei,0}$	m	SEI film thickness	$1{\cdot}10^{-8}$	